2017

Valproic acid: A neural outgrowth model for the autism spectrum disorder

Hannah M. Bergan
University of Northern Iowa

VALPROIC ACID: A NEURAL OUTGROWTH MODEL FOR THE AUTISM SPECTRUM DISORDER

An Abstract of a Thesis

Submitted

in Partial Fulfillment

of the Requirements for the Degree

Master of Science

Hannah M Bergan

University of Northern Iowa

December 2017

ABSTRACT

Autism spectrum disorder has been dramatically on the rise since the early 1990s, with one in forty-five children being diagnosed in 2014. It is known that contributing factors to autism spectrum disorder may have genetic and epigenetic origins, as well as environmental triggers. What is still unclear, however, is the impact of teratogenic drugs, consumed by the mother, have on a developing fetus *in utero*. How can they lead to the child developing autistic-like behaviors? The current study documents the effects of one teratogenic drug Valproic acid, a known histone deacetylase inhibitor. It establishes the role it plays on developing neurites and synapses within the brain. This study supports Markram's proposal of an "intense world theory" characterized by autistic-like behaviors due to hyper-functioning microcircuits within the brain. Dorsal root ganglia were dissected out of eight day old chick embryos, some of which were exposed to varying concentrations of Valproic Acid, to serve as a model for this study. The dorsal root ganglia were cultured for 48 hours and then underwent a three day immunostaining procedure in order for their neurites and synapses to be observed clearly under the microscope. Composite images of each dorsal root ganglia were constructed using the tiling program *ImagePro Premier*. This program was also then used to count neurites and measure their lengths. Another program *ImageJ* was used to measure the area of synaptogenesis. Dorsal root ganglia exposed to Valproic Acid developed more and longer neurites when compared to controls. When exposed to a specific concentration they began to develop larger synaptogenic areas. These findings support Markram's "intense world theory" in demonstrating that *in utero* exposure to

Valproic Acid may cause hyper-functioning synapses; begging to question as to whether or not other histone deacetylase inhibitors have the same effect.

VALPROIC ACID: A NEURAL OUTGROWTH MODEL FOR THE AUTISM SPECTRUM DISORDER

A Thesis

Submitted

In Partial Fulfillment

Of the Requirements for the Degree

Master of Science

Hannah M Bergan

University of Northern Iowa

December 2017

This Study by: Hannah M Bergan

Entitled: Valproic Acid: A Neural Outgrowth Model for the Autism Spectrum Disorder has been approved as meeting the thesis requirement for the

Degree of Master of Science

_____	_____
Date	Dr. Darrell Wiens, Chair, Thesis Committee
_____	_____
Date	Dr. Nilda Rodriguez, Thesis Committee Member
_____	_____
Date	Dr. Carl Thurman, Thesis Committee Member
_____	_____
Date	Dr. Patrick Pease, Interim Dean, Graduate College

ACKNOWLEDGEMENTS

This work would not have been possible without the help and support of my advisor, Dr. Darrell Wiens, and the University of Northern Iowa Biology Department. Nor without the support of my parents, Jane and David, who have always pushed me to try my hardest and never give up. Thank you.

TABLE OF CONTENTS

PAGE

LIST OF FIGURES

FIGURE PAGE

LIST OF TABLES

TABLE PAGE

CHAPTER 1

INTRODUCTION

Since the early 1990s there has been an evident increase in the number of children affected with autism spectrum disorder (ASD). There are many factors that may contribute to this increase including, but not limited to, genetic, epigenetic, and environmental conditions. Greater awareness and better diagnosis may explain some, but cannot explain the nearly exponential increase. This study investigates the epigenetic effects by examining the teratogenic drug valproic acid and its impact on embryonic neurons in culture. This approach should provide insight into one factor contributing to the etiology of autism at the cellular level.

Literature Review

Autism Spectrum Disorder

ASD can be defined as a complex developmental disability with symptoms typically appearing in early childhood that affects a person's ability to communicate and interact with others (Autism Society 2016). ASD has increased in prevalence among children, with cases jumping from one in two hundred-fifty reported in 2001 to one in forty-five in 2014 (Autism Speaks 2015). This data leads to the question as to what is causing this dramatic increase in the number of children reported with ASD. Certainly as technology and awareness of ASD advance, medical professionals are more apt to know the early signs and symptoms of ASD and are able to make improved diagnoses. Yet it is improbable that this accounts for all of the increase. Signs and symptoms of autism can

be divided into five categories: behavioral, developmental, cognitive, psychological, and other. 1) Behavioral signs include inappropriate social interaction, poor eye contact, compulsive behavior, impulsivity, repetitive movements, self-harm, and persistent repetition of words or actions. 2) Learning disabilities or speech delay are examples of developmental symptoms. 3) Intense interest in a limited number of things or problems paying attention fall under cognitive symptoms. 4) Psychological signs include unawareness of others' emotions or depression. 5) Other signs include but are not limited to anxiety, change in voice, excessive sensitivity to sound, or a tic (summarized from the CDC 2015). There is no known single cause for autism, but evidence supports involvement of genetic and epigenetic factors. This paper will focus on epigenetic factors that may lead to hypo- and hyper-connectivity of neurons in the developing brain.

Valproic Acid

Valproic Acid (2-n-propyl pentanoic acid, VPA) is a medication primarily used to treat epilepsy and seizures, but also as an antipsychotic for bipolar disorder, and migraine treatment. It may also be used to treat children with attention-deficit/hyper-reactivity disorder (ADHD). VPA has known teratogenic effects and has been linked to malformations in humans and other animals when exposed *in utero*, a configuration of symptoms known as fetal valproate syndrome (FVS) in humans (DiLiberti et al. 1984). FVS is reported as showing congenital malformations, dysmorphism and abnormal neurological signs at birth (Laegreid et al. 1993). Larger studies have provided evidence that VPA exposure and the development of FVS *in utero* may be linked to an increased

risk of ASD, reporting the rate of ASD to be eight times larger in VPA treated mothers than the general population (Rasalam et al. 2005).

The "Intense World Theory"

The "intense world theory" of ASD can be described as excessive neuronal information processing and storage in the microcircuits of the brain that can produce hyper-perception, attention, and memory in those affected. The cause of excessive processing may be attributed to hyper reactivity and plasticity of the microcircuits including hyper-connecting neighboring neurons producing excessive excitation as well as hyper-expressing N-methyl-D-aspartate (NMDA) receptors producing excessive plasticity in the neocortex. The microcircuits may then become increasingly difficult to control and coordinate with other microcircuits when activated (summarized from Markram et al. 2007). The hyper-functioning of microcircuits is expressed physically as it produces outward signs including decreased social interactions, excess sensitivity to pain, increased sensitivity to non-painful stimuli, repetitive activity, increased anxiety and high and longer fear memories that are harder to extinguish (Ebert and Greenberg 2013). These outward signs correlate with many of the symptoms of ASD.

Rodent Model

Rodent models of ASD have frequently been used in research in order to exhibit the behavioral and neurological effects of prenatal VPA exposure. In a study performed by Schneider and Przewlocki (2004) rats were exposed to VPA on the 12.5 day of gestation with offspring's social behavior being examined in adulthood. Their findings included a lower sensitivity to pain with higher sensitivity to non-painful stimuli,

diminished acoustic pre-pulsed inhibition, repetitive and lower exploratory activity, and a decreased number of social behaviors (Schneider and Prezwlocki 2004). These behaviors can all be placed into one of the five categories listed above as typical signs and symptoms of ASD in children.

Another study (Go et al. 2012) examined neuronal developmental effects of prenatal VPA exposure in rats. One of their findings was induced macrocephaly with prenatal exposure to VPA. This corroborates previous studies that found enlarged brain circumference in patients exhibiting ASD and FVS (Yoo et al. 2002). Go and colleagues also reported an increase in the proliferation of neural progenitor cells (NPC) resulting in a delayed, but eventual increase in the number of differentiated neurons. Affected cortical areas showed increased thickness, signifying that numbers of excitatory neurons may also be increased along with total number of neurons. Increasing excitatory neurons with or without affecting (but leading to a down-regulation) inhibitory neurons would be enough to induce abnormal behavior such as repetitive and restricted behaviors, and also low pre-pulse inhibition, as mentioned above from the previous study of Schneider and Przewlocki (2004) (summarized from Go et al. 2012).

Investigating further effects on neurons, Mi Ra Jeong and colleagues (2003) reported a study in which they harvested and cultured cortical neurons (CCN) from 17 day old embryonic rats and treated them with 0.1-1 mM VPA starting at day 9 *in vitro*. CCNs not treated with VPA underwent spontaneous cell death with increasing age. However, VPA treated CCN's spontaneous cell death was noticeably suppressed, suggesting a neuroprotective effect of VPA. This was accompanied by a more than two-

fold increase of histone H3 acetylation, suggesting an inhibition of histone deacetylases (Jeong et al. 2003).

Mechanism of Action

There is no single mechanism of action for VPA as it dissociates into valproate ions leading to multiple effects on neuronal tissue in the brain. VPA increases brain concentrations of GABA (gamma-aminobutyric), an inhibitory neurotransmitter, which prevents seizures. However, VPA is also thought to enhance the effects of pre-existing GABA on its receptors and on NMDA glutamate receptors, also contributing to its anticonvulsant effect (summarized from Smith 2015).

Histone Deacetylase Inhibition

VPA is a known histone deacetylase (HDAC) inhibitor. Histone deacetylases are important in regulating gene transcription and phenotype expression by functioning as transcriptional repressors. HDACs have also been shown to act on many cellular substrates as well as on histones, demonstrating that acetylation may rival phosphorylation in importance (reviewed by Haberland et al. 2009). HDACs can be separated into two classes: HDACI and HDACII. MacDonald and Roskam (2008) observed that HDACI is expressed in neural stem cells/progenitors, but as they exit the cell cycle HDACI expression is lost. Expression of HDACI is however maintained in glia throughout the cell cycle. HDACII is initiated in postmitotic neuroblasts and neurons, and upregulated as they commit to a neuronal lineage, but is not expressed in fully differentiated glia. Studies have suggested that HDACI may contribute to fate decisions and lineage commitment and be a prominent player in deacetylation during glial

development. On the other hand, HDACII may contribute to the regulation of subsets of neuronal genes during the differentiation of neurons (MacDonald and Roskam 2008). A study done by Akhtar and colleagues (2009) used electrophysiological, immunocytochemical, and optical methods to demonstrate that HDACI- and HDACII-mediated chromatin silencing restricts the progression of excitatory synapse maturation during early synapse development. They suggest that the chromatin state maintained by HDACs suppresses excitatory neurotransmission when synapse formation is sparse, but augments excitation when neuronal networks mature and synapses are in abundance (Akhtar et al. 2009). Immature neural networks may have an enhanced vulnerability to HDAC inhibition leading to prominent increases in the structural assembly of synapses and growth of neural networks (Chomiak et al. 2013).

VPA accomplishes HDACI inhibition by binding to its catalytic site and blocking substrate access. However it inhibits HDACII by inducing proteasomal degradation (Chomiak et al. 2013). Phiel and colleagues (2001) also reported that VPA acts as a HDAC inhibitor. They proposed that HDAC inhibition by VPA activates Wnt-dependent gene expression that leads to increased expression of β-catenin and de-repression of Tcf/Lef (group of transcription factors involved in the Wnt signaling pathway). This can lead to the over-connectivity and hyper-excitability described in the intense world theory (Phiel et al. 2001).

Histone Methylation

As is the case with histone deacetylation, histone methylation is an important epigenetic function for regulating gene transcription, developmental gene programs, and cellular phenotype (Chomiak et al. 2013). Histone lysine methylation occurs on histones H3 and H4 and they can be mono-, di-, or tri-methylated. Depending on the site of methylation it can signal either activation or repression. It is speculated that methyl-H3-K4 and methyl-H3-K9 are binding sites for proteins that mediate the biological effects of histone methylation modifications (Martin and Zhang 2005). It is accepted that the tri-methylation of histone H3-K4 is very important for transcriptional activation at promotor regions (Mosammaparast and Shi 2010), whereas methylation of H3-K9 may act to silence genes (Berger 2007).

In order to examine the effects of VPA on histone methylation and subsequent gene expression, Tung and Winn (2010) exposed pregnant mice to 400mg/kg VPA and collected their embryos at successive stages after injection with VPA. They then examined the effects on histone methylation. They observed a significant decrease in the expression of monomethyl histone H3-K9 and a significant increase in the expression of di- and tri-methylated histones H3-K4 suggesting a shift towards more active gene expression in the embryos (summarized from Tung and Winn 2010).

Rinaldi and colleagues (2007) exposed rat pups prenatally to VPA in order to investigate alterations made to the glutamatergic system and its second messenger pathways. They found an overexpression of NMDA receptor subunits leading to enhanced NMDA receptor-mediated synaptic currents and amplified postsynaptic

plasticity in neocortical pyramidal neurons (Rinaldi et al. 2007). NMDA receptors regulate the expression of brain-derived neurotrophic factor (BDNF). An overexpression of NMDA receptors leads to an overexpression of BDNF, which in turn increases dendritic growth in neurons (Horch and Katz 2002).

Dorsal Root Ganglia

Vertebrate embryos form a transient ectodermal structure known as the neural crest from which a subpopulation of migratory neural crest cells (NCCs) emerges. An epithelial to mesenchyme transition (EMT) facilitates the migration of NCCs from the dorsal neural tube outward through the extracellular matrix towards remote target destinations where they differentiate into a wide array of diverse tissues.

In one such differentiation, NCCs develop into the dorsal root ganglia (DRG). The NCCs that form DRGs migrate a short distance through anterior somite tissue and then settle segmentally in clusters to differentiate as bipolar neurons and glia. As they continue to develop, DRGs send neural processes outwards to form junctions at target tissues and also inward medially to the spinal cord. The DRGs contain the greatest proportion of sensory neurons that transmit information from the periphery into the central nervous system (Krames 2014) which can be explanted to tissue culture to create an experimental model of neural outgrowth (Cohen et al. 1954; Levi-Montalcini 1964; Letourneau 1975). Once adhered in their target tissue a neural network forms and neurites begin to extend outward to form synaptic networks which can be detected by immunostaining with an SV2 antibody (Wiens et al. 2016). A neurite is defined as any projection from the body of a nerve cell (neuron), either an axon or a dendrite (Collins

English Dictionary). Growing axons then navigate through the cellular terrain and associated extracellular matrix to find appropriate synaptic partners. They accomplish this through the use of growth cones, a specialized structure at the tip of growing axons, first discovered by Harrison (1910). The morphology of a growth cone is a sheet-expansion of the growing axon at its tip called a lamellapodium with many fine processes called filopodia that extend and retract to sense the environment and afford transient adhesion sites. Growth cones explore the extracellular environment in order to determine the direction of growth and guide the axon's extension in that direction (Purves et al. 2001). There are three important families of molecules that guide growth cones to their target destinations. The first, cell adhesion molecules, reside on cellular surfaces and extracellular matrix substrates along the path the growth cone is traveling and are recognized by specific receptors on the growth cone's membrane. Once contact has been made, other signals are transmitted to the cytoplasm and set the direction for growth cone adhesion and motility. The second family contributing to growth cone guidance are diffusible molecules that guide the growth cone through chemotaxis by diffusing freely into the aqueous environment surrounding the growth cone. They may either attract or repel the growth cones. The third family consists of growth (trophic) factors that are also small diffusible molecules but act more generally to stimulate elongation of the axon and the formation of synaptic connections (McGill 2013).

Hypothesis

Because VPA is known to mimic ASD in rodents by altering brain development via epigenetic dysregulation (Chomiak et al. 2013), it is important to examine its effects directly on the developmental cellular behavior of neurons. One suitable experimental system that can be used to examine this is DRG neurons in culture (Wiens et al. 2016). Therefore I have used immunostaining procedures and microscopic image analysis to investigate the neurites, growth cones, and neural networks of DRGs in eight-day-old chick embryos treated with increasing concentrations of VPA. I have compared them to untreated controls. As previous studies suggest, VPA should stimulate some or all neurogenic activities. Therefore, I expect to find an increase in neurite number and length with an increase in area of synaptogenesis in treated DRGs compared to controls.

CHAPTER 2

MATERIALS AND METHODS

Dissection and Culture

Fertile chicken eggs were purchased from Mixdorf farms (Waterloo, IA) and incubated at 38˚C for eight days. The method for dissection and culture of the DRGs by Wiens et al (2016) was followed. On the eighth day embryos were extracted from the eggs and transferred to a petri dish containing Earle's Balanced Salt Solution (EBSS) (Sigma-Aldrich). Each embryo was then placed into a sterile dish under a binocular microscope for dissection. The head and internal organs were removed in order to expose the spinal cord. Then, microscissors (Minitool, Inc., Los Gatos, CA) were used to sever the dorsal roots and excise the small, ovoid DRGs from their location near the spinal cord. A micropipette was used to transfer them out of the dish into a second sterile dish of EBSS. Twenty-five to thirty DRGs were typically collected from each embryo and the dish was then carefully transferred to a laminar flow hood to prepare the DRGs for culture. Five to six DRGs were transferred via micropipette from the EBSS into Falcon Primaria 35 mm diameter culture dishes (Fisher Scientific) to ensure that two or more would attach. Excess EBSS was removed and 2 mL of Medium 199 (Sigma-Aldrich), supplemented with 10% fetal bovine serum (MP Biomedicals, Santa Ana, CA) and 1% antibiotic/antimycotic solution (CellnTec, Bern, Switzerland) was added to each dish. Either 1, 2, 4, or 6 µL of VPA (2-propylpentanoic acid, Sigma-Aldrich) was added to the experimental dishes from a 2.0 M stock solution to achieve final concentrations of 50, 100, 200, or 300 µM. Control dishes received equivalent volumes of medium only.

The dishes were then incubated at 38 °C with 5% CO_2 and 100% humidity for 36-48 hours. Attachment was observed by 24 hours for all conditions, and those explants not attached were excluded from the experiment.

Fixation and Immunostaining

Following culture the DRGs were taken out of incubator and the dishes were immediately placed on ice in order to stop neural outgrowth and development. The medium was then pipetted out and replaced with EBSS briefly to wash, and then 1 mL of ice cold 20% DMSO in methanol was pipetted into the dishes on ice for one hour with gentle agitation in order to fix the DRGs. The method for the immunostaining of fixed DRGs was the method of Wiens et al (2016). Briefly, after one hour of fixation, the cultures were washed with a phosphate buffer saline (PBS) solution three times for two minutes each. A peroxidase quenching solution (3% H_2O_2 in methanol) was added to the dishes for ten minutes followed by 3 PBS washes. The cultures were then permeabilized with gentle agitation for thirty minutes in 0.1% Triton X-100 in PBS followed by 3 more PBS washes. Blocking solution (0.5% Tween-20, 2.5% bovine serum albumen, 0.5% nonfat dry milk in PBS) was then added for one hour with gentle agitation. Mouse monoclonal antibody SV2 (Developmental Studies of Hybridoma Bank, University of Iowa Department of Biological Sciences, Iowa City, IA) secreted into culture solution was added to the blocking solution in a 1:20 dilution and incubated at 4°C overnight. The next day the cultures were warmed to ambient temperature with gentle agitation. The antibody-blocking solution mixture was removed and they were washed three times in PBS. Biotinylated anti-mouse IgG from a Histostain SP kit (Invitrogen) was added to

the dishes for 20 minutes followed by PBS washing three times and then streptavidin-peroxidase conjugate solution, also from the kit, was added for 15 minutes with gentle agitation followed by PBS washing 3 times. A chromagen mixture containing 1% 3-amino-9-ethylcarbazole and 0.3% H_2O_2 in 0.05M acetate buffer was placed on the cultures and allowed to develop in darkness for 10 minutes after which antibody-positive DRGs were stained red. This was then removed and the cultures immediately rinsed with dH_2O to stop the reaction. The stained cultures were then post-fixed in 3.7% paraformaldehyde solution at 4 °C for eight minutes to stabilize the red color. The cultures were then rinsed and stored in the refrigerator in dH_2O.

Seven control DRGs were also immunostained in the same way but without addition of the primary antibody. Without adding primary antibody, the chromagen mixture could not adhere to synaptic vesicles and thus not stain red. This showed that the immunostaining procedure was successful and that no non-specific binding occurred.

Image Analysis in *Image Pro Premier*

Image composites and neurite and growth cone measurements were made using *Image Pro Premier* software (Media Cybernetics, Inc., Rockville, MD). The culture dish was placed on the stage of a Leica DMIRE-2 inverted microscope with Q-Imaging CCD camera (Surrey, BC, Canada) attached and the DRG of interest was located and adjusted into focus using differential interference contrast optics on the screen of a Dell Optiplex 980 computer. Commands in the *Image Pro Premier* program were then used to tile the DRG with the 10x objective of the microscope in position until a composite image was created. This was then saved as a .tiff image. Image tiling refers to capturing multiple

images at an increased magnification and then aligning and joining them in order to create one composite image. After the DRG images had been tiled and saved they were opened again in *Image Pro Premier* to count and measure neurites. Before beginning the measurements the program was calibrated from pixels to micrometers using a section of ruler that had been tiled as before and setting the scale in the software. A tiled image was then opened and twelve radial lines were drawn at successive 30° angles from the center of each explant (Figure 1). Any neurite touching or crossing a line was counted and measured for length by using the mouse to trace it from where it began at its corresponding cell body or dendrite to where it ended at either another cell body or in the field of view. This ensured a selection of a random representative sample. The numbers given for length were then divided by two because the *Image Pro* program was increasing the number of pixels during tiling by overlapping the joined images. This number was determined by comparing an uncalibrated tiled image to an image that was calibrated before and during tiling to compare pixels per unit. Multiple explants were tested this way to give an average ratio of 0.5, thus dividing all initial measurements in half. The measurements were then saved in a Microsoft Excel file for further analysis.

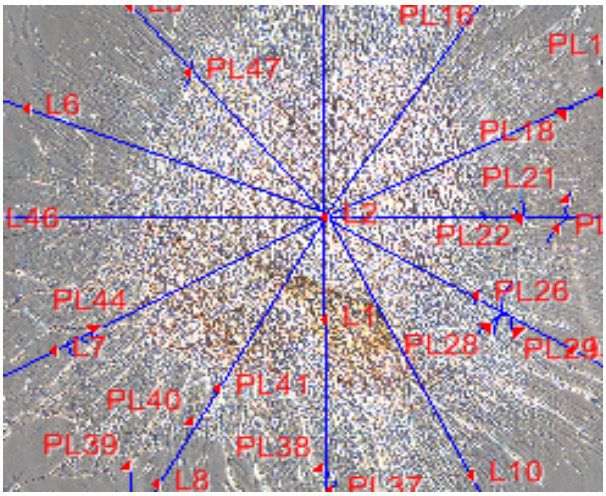

Figure 1. Composite image of a DRG showing a dense neuronal network. Random assessment was achieved by only counting and measuring neurites that touched or crossed any one of the twelve lines shown drawn at 30° angles from the center of the explant. (All markings shown as "PL" indicate neurites traced).

Image Analysis in *ImageJ*

The red stained area of synaptogenesis was measured using the color thresholding feature in the program *ImageJ*. First, the program was used to cut out the central DRG original explant (Figure 2). This was necessary because of its 3-dimensional complexity that made color thresholding inaccurate. Furthermore, the aim was to assess synapse formation among neural connections that had been created during the period of culture, and these were peripheral. There was a definite visible depth change among cells at the explants' edge which was used to determine the border of the explant to cut out. The color thresholding option of *ImageJ* was then used to find the total area of all the pixels above a computer-determined level of red intensity. The total

area was then divided by two to account for the overlapped images created during tiling. It was also necessary to account for the variation in size of the explants. A larger explant will have a larger synaptic area by default. This was done by measuring the largest diameter of the cleared portion of each explant, finding the average of these, and dividing the average by each diameter. This gave a diameter quotient that we used to adjust each peripheral area measured. The corrected areas were lastly divided by their respective diameter quotient to end with our area of synaptogenesis in square microns used for analysis.

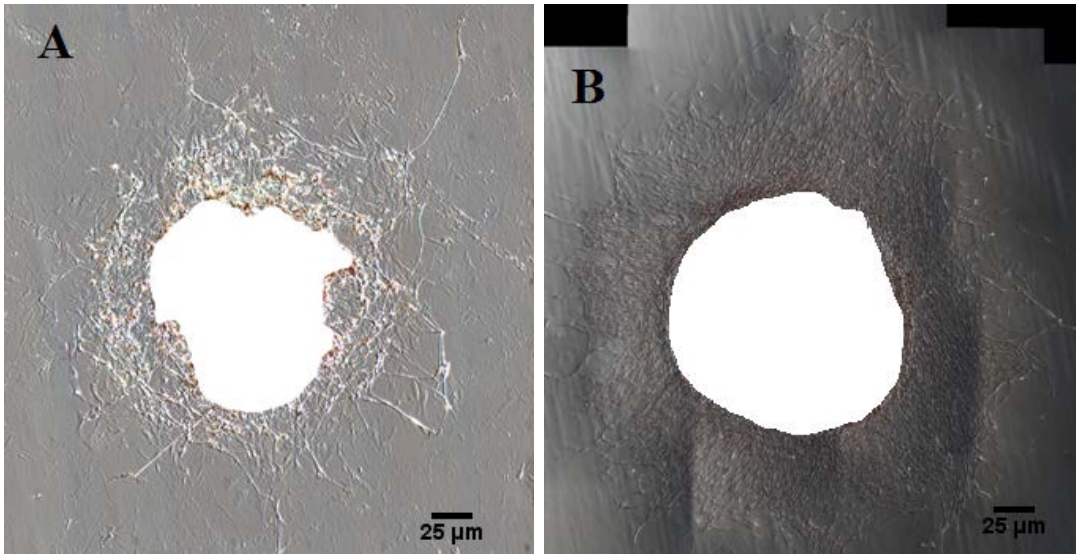

Figure 2. Composite images of cultured DRGs in *ImageJ* program. A) Control DRG with the central DRG cut out to measure synaptogenic area around peripheral edges. B) DRG exposed to 100µM concentration of VPA with the central DRG cut out to measure synaptogenic area around peripheral edges.

Statistical Analysis

The raw measurements for the neurites were initially saved in *Excel* files and then sorted and saved as CSV files for further analysis. R language for statistical computing (R Core Team, 2012) was used to create histograms and boxplots of the data. Significance values for neurite length and synaptogenic area were $p \leq 0.05$ and were computed in R using the Wilcoxon Rank Sum Test because the histogram data analysis showed the values were not normally distributed. Histogram data for neurite number showed normally distributed values, so significance was computed using a T-TEST in Microsoft *Excel*. The histograms can be seen in Appendix A.

CHAPTER 3

RESULTS

In this study, I carried out experiments in order to observe if there was evidence that the pharmaceutical valproic acid may cause increased neuronal outgrowth, thus leading to an increased risk for the development of ASD. The DRGs of eight-day-old chick embryos were used as my model for analysis. DRGs develop along the spinal cord in both chicks and humans, as part of the peripheral nervous system, and feature neurons that extend neurites led by growth cones during their development. The growth cones eventually establish synaptic connections both with receptors peripherally and also within the developing spinal cord. Immunostaining and image analysis techniques were used to evaluate both unexposed (control) DRGs and DRGs exposed to varying concentrations of VPA. At the time of dissection, the DRGs are lined up along the spinal cord, ready to innervate target tissues. In culture, they adhere to the treated, charged plastic culture dish and spread outward. Monoclonal antibody SV2 was used to detect and measure the extent of differentiating synaptic networks.

Developmental Progression and Staining Specificity

The DRGs attached to the culture dish within a few hours. This was accompanied by the appearance of early migrating fibroblasts at the peripheral edges. Following these cells and mainly using them as a migration substrate, neurons with thick cell bodies (recognizable by their phase halos) and neuronal processes (neurites) began to extend outward in all directions. Their neuronal processes lengthened, led by growth cones, and they then began to form synaptic networks. Between 40 and 48 hours of

culture, the neurites began to assemble into “nerves” that were thicker than neurites, and consisted of multiple neurites in bundles.

Immunostaining was performed using both primary and secondary antibodies in order to locate the development of synaptic networks around the explants. Synaptic networks stained red indicating the presence of neuronal structures having synaptic vesicles (Figure 3, B and C). This included cell bodies, neurites and growth cones as well as maturing synapses, as these areas contained differentiating components of synaptic vesicles (Figure 3, D). In order to exclude non-specific binding of the antibody, nine explants were taken through all steps of the immunostaining procedure, but were not exposed to the primary mouse monoclonal SV2 antibody. The secondary anti-mouse biotinylated antibody binds to the primary, so without it no red color should be observed. In our case, no red color was observed, indicating little or no non-specific binding of the antibody (Figure 3, A).

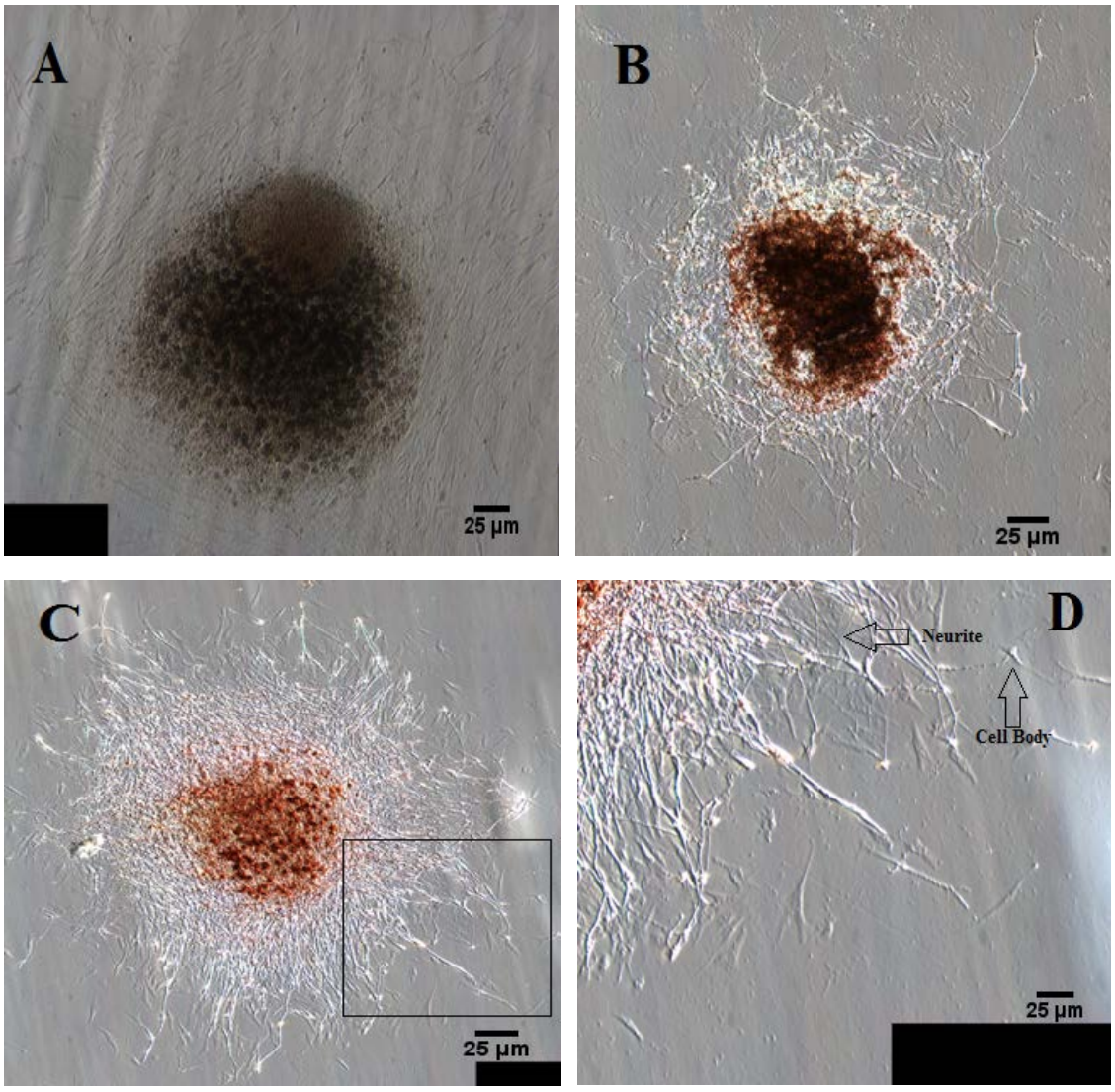

Figure 3. Composite images of cultured DRG explants after 48 hr. of culture. The original DRG lies elevated somewhat at the center of a spreading layer of cells. Elongated neural processes (neurites) are indicated by arrows. A) A no primary antibody control showing no red stained areas. B) An immunostained control DRG showing its neuronal network. C) An immunostained DRG exposed to 100µM VPA concentration, showing a more extensive neuronal network. D) Enlarged area shown inside the box of C showing matured synapses with clear cell bodies and neurites that had developed during culture.

The Effect of Valproic Acid on the Number of Neurites

The DRGs transferred to Primaria culture dishes attached to the dish surface within the first day of culture and a neuronal network began to grow outward in all directions from the explant. Explants were removed from culture after 48 hours and immunostained as described above. Image analysis was performed to examine the neuronal networks. Noticeable among them were very thin, straight cell processes that could be traced back to a larger cell body (neuron) and we identified these as neurites (Figure 3, D). All statistical data accumulated is based on the averages of all neurites counted for number and measured for length and area for each respective experiment. The number of DRGs collected and analyzed for neurite number and length was 31 control DRGs, 8 50 µM VPA DRGs, 36 for 100 µM VPA DRGs, 10 for 200 µM VPA DRGs, and 9 for 300 µM VPA DRGs. The average number of neurites per DRG for each group is shown in Figure 4. The complete data set is given in Table B1, Appendix B. A histogram plot of this data showed a normal distribution (Appendix A, A1). Therefore, a T-TEST was used to determine whether differences were significant. All of the treated explants, except those treated with 50 µM VPA, showed a significantly larger number of neurites than controls. However, the treated explants did not differ significantly from one other. All significance values can be seen in Table C1, Appendix C.

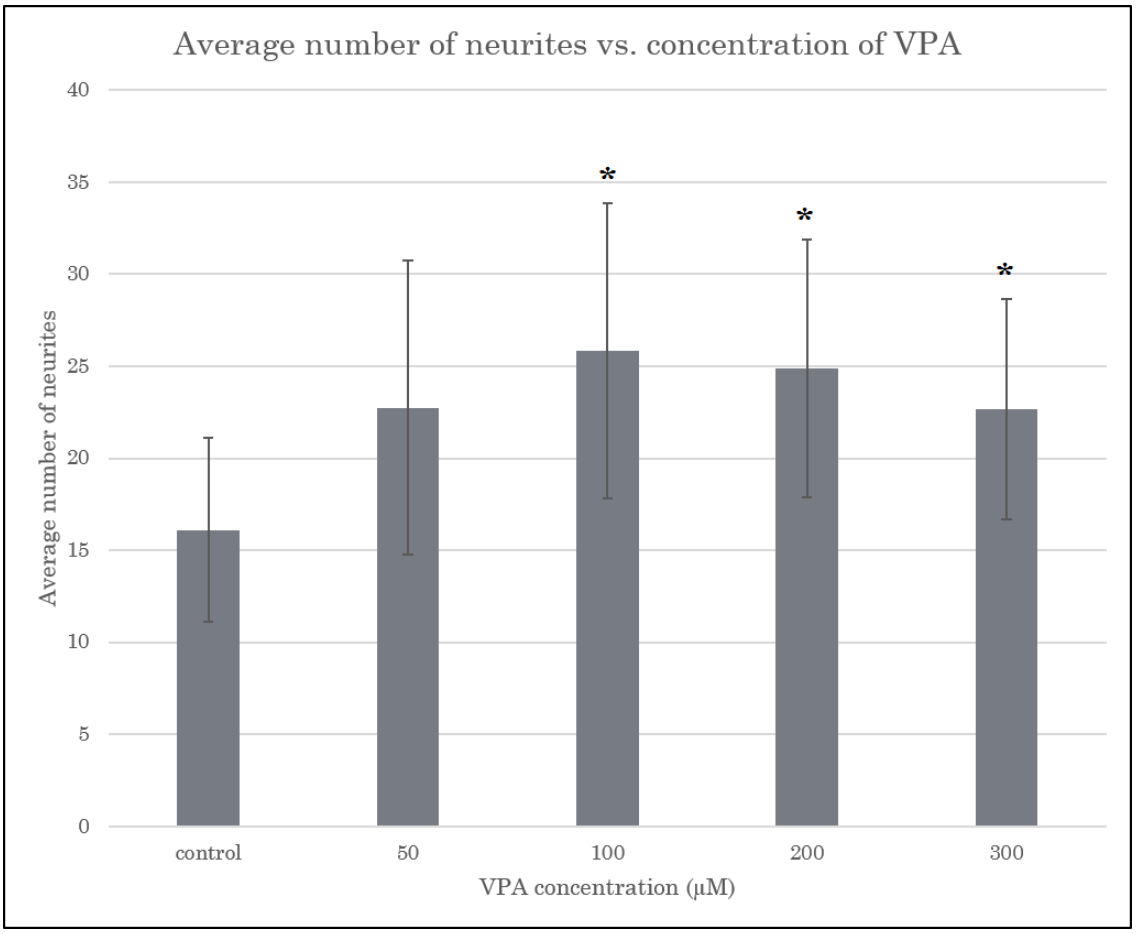

Figure 4. Average number of neurites ± standard deviation found in each 12-line random sample taken from the indicated number of DRG explants. Treatment with VPA resulted in a greater number of neurites per explant. Error bars show standard deviation. Asterisks represent significance when compared to the controls with $p \leq 0.05$.

The Effect of Valproic Acid on Neurite Length

As described above, neurites were counted based on whether they touched or crossed one of the twelve sample lines (Figure 1). Once each such neurite was located, its length was measured from where it began at the cell body to where it ended at a corresponding cell body or in the field of view. These were traced using a computer mouse and length measurements were generated by the *Image Pro Premier* software in microns after calibration had been applied. After all analysis was completed, the measurements generated by the software were each divided in half to make up for the extra pixels created during tiling. The average length of neurites per DRG was 54 µm for the control, 71 µm for 50 µM VPA, 112 µm for 100 µM VPA, 74 µm for 200 µM VPA, and 71 µm for 300 µM VPA. The complete data set is given in Table B2, Appendix B. A histogram was created for the data set which showed a non-normal distribution (see Appendix A, A2). This is because the outgrowth of the explants neuronal networks was radial, therefore there were many more, shorter neurites closer to the edge of the explant. Thus, lengths tapered oppositely and rapidly with distance from the edge, and these taperings led to the non-normal distribution (Wiens et al. 2016). Since the data was not normal, the Wilcoxon Rank Sum Test was used to analyze significance as it accounts for the non-normally distributed data. The Wilcoxon test showed many significant differences, most prominently that all treated explants developed neurites that were significantly greater in length than controls. When compared to each other, neurites from explants treated with 100 µM VPA were significantly longer than those from explants treated with 50 µM, 200 µM or 300 µM VPA. Unexpectedly, explants treated with either

200 µM or 300 µM VPA were *not* significantly longer than those treated with 50 µM VPA and there was no significant difference in length between those treated with 200 µM and 300 µM VPA (see Table C2, Appendix C for all significance values). Figure 5 displays a graphic summary of these results.

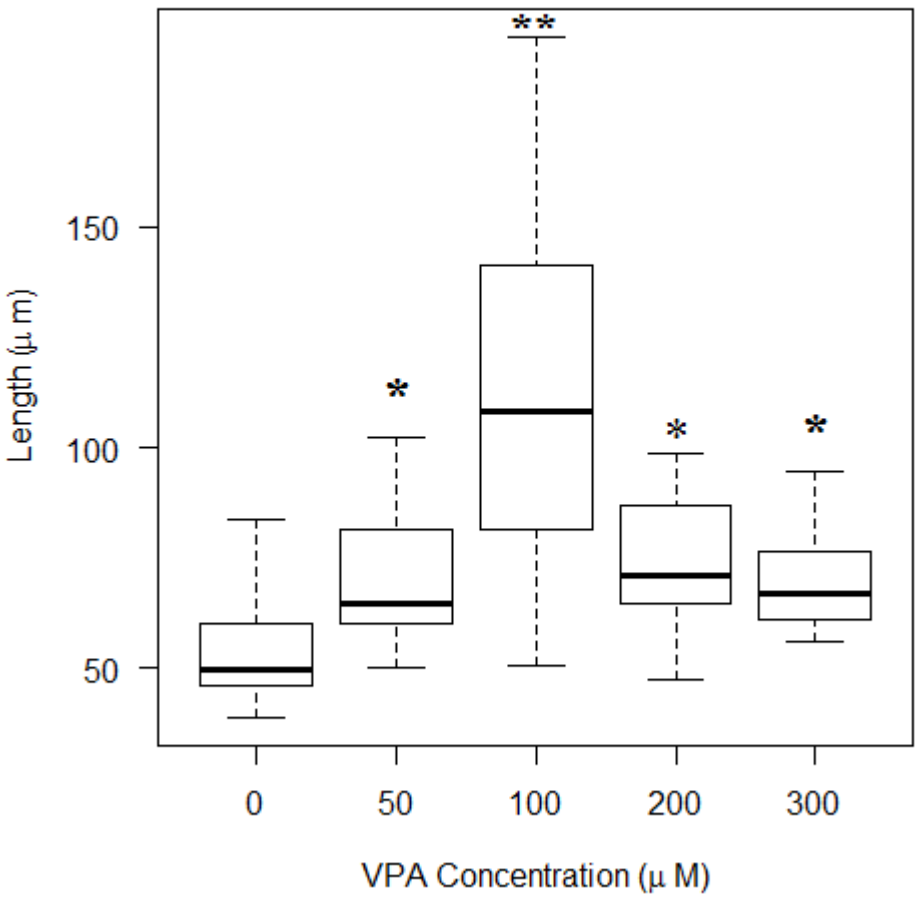

Figure 5. Boxplot of data depicting lengths of neurites collected from a random sample around explants. Treatment with VPA resulted in neurites with greater lengths when compared to untreated explants with a maximum effect with 100 µM VPA. A boxplot of the data is seen here. Boxes represent data measured from 31, 8, 36, 10, and 9 explants respectively. The heavy black lines represent median lengths, lower end of the boxes represent first quartiles, upper end of boxes represent third quartiles, and whisker's show maxima and minima neurite lengths. Significance analysis showed all lengths being significantly greater than those of control explants and are represented as $p \leq 0.05$ with an asterisk. The concentration at 100 µM has significance indicated with a double asterisk, for neurite length at that concentration was significantly greater when compared to controls and to the other concentrations. See Table C2, Appendix C for all significance testing.

The Effect of Valproic Acid on the Area of Synaptogenesis

Area of synaptogenesis around the DRG was also analyzed. It was expected to increase among those explants treated with VPA. The SV2 antibody used during the immunostaining procedure specifically binds to synaptic vesicles and their precursor molecular components assembled in neurons around the DRG. The middle of the explant was clearly and prominently stained red due to a very high concentration of synaptic vesicles in that area. However, because of the high density and three-dimensional arrangement of neurons there, staining was difficult to evaluate accurately. Also, our aim was to assess the synapses formed during culture, therefore, we restricted analysis to the circumference of the explant. Before beginning analysis we carefully traced a border around the body of the explant. The border was drawn around those cells which had not migrated outward and this could be seen as a noticeable depth change of the cells (Figure 2). Area measurements were then generated in square microns by *ImageJ* Software with corrections for pixels and DRG shape accounted for as described in Methods. 10 control DRGs, 8 50 µM VPA DRGs, 10 100 µM VPA DRGs, 10 200 µM VPA DRGs, and 9 300 µM VPA DRGS were measured for their amount of red-stained synaptogenic area. The average stained area of explants was 8113 μm^2 for the control, 10641 μm^2 for 50 µM VPA, 12119 μm^2 for 100 µM VPA, 10040 μm^2 for 200 µM VPA, and 13148 μm^2 for 300 µM VPA. A complete data set is shown in Table B3, Appendix B. A histogram was created for the data set and showed non-normal distribution (see Appendix A, A3), so the Wilcoxon Rank Sum Test was used to test for significance. Explants treated with 300 µM VPA had a significantly larger synaptogenic area than controls. All other

comparisons were not found to be significantly different (see Table C3, Appendix C for all significance values). Figure 6 below displays a graphic summary of these results.

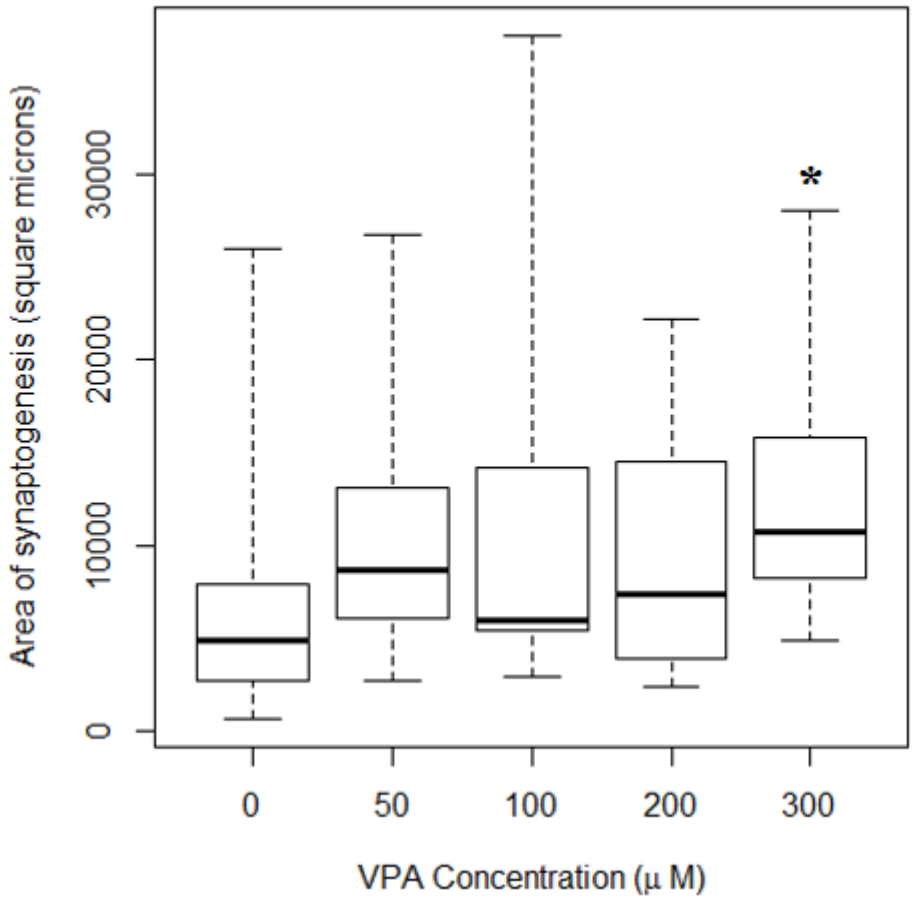

Figure 6. Boxplot of the data depicting area of synaptogenesis in square microns of area around the explants. Treatment with VPA resulted in larger synaptogenic areas around the explant when compared to untreated DRGs. Boxes represent data measured from 10 controls, 8 50 µM VPA, 10 100 µM VPA, 10 200 µM VPA, and 10 300 µM VPA DRGs. Treatment with 300 µM VPA resulted in a significantly larger area of synaptogenesis with $p \leq 0.05$ and is shown with an asterisk. Thick black lines represent median, bottom portion represents first quartile, top portion represents third quartile, and whiskers represent maxima and minima areas. (See Table C3, Appendix C for all significance testing values).

CHAPTER 4

DISCUSSION

Valproic acid is a pharmaceutical primarily used to treat seizures due to its strong anti-epileptic properties that involve reducing neuronal activity by blocking sodium and calcium channels and by enhancing the function of GABA, an inhibitory neurotransmitter. However, maternal ingestion of VPA during pregnancy may have profound teratogenic effects on the developing fetus which are associated with a 3-fold increase in the rate of major malformations (Kataoka et al. 2013). Also, VPA ingestion while pregnant may lead to an increased risk of development of autism-like behaviors in children. This occurs mainly because of increased histone acetylation leading to hyper-connected neural networks in the brain. In this study, I modeled neurogenesis using DRG explants from eight day old chick embryos and exposing them to increasing concentrations of VPA. This allowed for the examination of neurons at the cellular level including the formation of neurites led by growth cones and neural network formation. At day six of incubation neurons of DRGs in the chick embryo initiate neurites to innervate the spinal cord and connect to peripheral receptors. Therefore neurogenesis begins and accelerates at a time when the same neurogenic events are underway in the brain and spinal cord. At day eight of incubation, DRGs can be easily dissected from the spinal cord and cultured.

My results demonstrated that DRGs exposed to VPA initiated more neurites that were longer when compared to control. This enabled the development of larger neural networks. These findings strengthen the current hypothesis that VPA exposure leads to

hyper-excitable neural networks in a developing fetus leading to an “intense world” characterized by autistic-like behaviors (Markram et al. 2007).

My dose-dependent findings showed a maximum effect on neurite length and number for those DRGs treated with 100 µM VPA. There are a couple of reasons as to why this could have happened. There were 36 DRGs that were exposed to 100 µM VPA, whereas there were only 10 DRGs exposed to 200 µM VPA and 9 DRGs exposed to 300 µM VPA, therefore the data could be slightly off. Another possible reason for this could be that at exposure to 100 µM VPA activates complete histone deacetylase inhibition and displays its maximum effect. When the DRGs were exposed to 200 µM and 300 µM the increase in neurite number and length was still significantly higher than controls, but not 100 µM concentration. This could also be due to VPA inducing a saturable effect, where increasing concentrations of the chemical do not continue to increase neurite number and length. The effect for number and length seem to level off at 100 µM, but the area of synaptogenesis data continues to rise with a maximum and significant effect at 300 µM VPA. The biological processes measured were different ones therefore it is possible that neurite number and length have a maximum response at 100 µM, but the synaptogenic area will continue to increase with increasing concentrations of VPA. In order to resolve what is happening here, further research should be executed.

The activity of histone deacetylases is an important factor in the regulation of genes associated with chromatin condensation. It has been shown that HDAC1 is required to switch neural progenitor cells (NPC) from proliferation to differentiation in the developing vertebrate retina, and a mutant model of HDAC1 failed to do so therefore

proliferation of NPCs was increased (Go et al. 2012). By inhibiting the epigenetic activity of histone deacetylases a group of genes may be turned on that would result in the increased number of neurites found in this experiment. One such mechanism is the selective overexpression of the ionotropic NMDA receptor subunits NR2A and NR2B. Rinaldi and colleagues (2007) performed a study in 2002 that involved prenatally exposing rats to VPA and monitoring the changes in glutamate mediated synaptic transmission and plasticity in the neocortex. They found that ionotropic NMDA receptors are the key receptors underlying synaptic plasticity in the neocortex, so their data suggests that an important aspect in VPA exposure is related to synaptic plasticity. These authors also reported that Calcium/Calmodulin-dependent protein kinase II (CAMKII) is the second messenger most closely linked to ionotropic NMDA receptors, and was also found to be overexpressed in VPA treated rats. CAMKII mediates synaptic plasticity, experience-dependent synaptic changes and memory. CAMKII also mediates the postsynaptic form of long-term potentiation or LTP (an increase in synaptic strength following stimulation of a chemical synapse) and has also been found to be enhanced in VPA treated rats. The overexpression of these receptors translates into enhanced NMDA receptor-mediated synaptic currents and an amplified postsynaptic form of synaptic plasticity in the neocortex. Their results suggest molecular and synaptic alterations in children prenatally exposed to VPA (Rinaldi et al. 2007). My findings showed an increase in average neurite number, length, and in synaptogenic area. This leads us to believe that HDAC inhibition is a leading mechanism of action in the neural networks of children exposed to VPA *in utero*.

It has also been shown that enhanced activity of the NR2A subunit can lead to increased brain-derived neurotropic factor (BDNF) expression, which is important in neuronal development as it has been shown to increase the number of basal dendrites (Horch and Katz 2002). A study done by Yoo and colleagues (2016) looked at effects of increased expression of BDNF on neurogenesis in mouse brains. They found increased neurogenesis and neurite outgrowth during the early developmental stages of mice with an overexpression of BDNF (Yoo et al. 2002). Our results showing the increased neurite number, length and area in VPA exposed DRGs are consistent with Yoo's findings, indicating a possible mechanism by which this is happening. Yoo and colleagues (2002) also found an increased brain size in mice exhibiting BDNF overexpression, which was correlated with ASD in its early years of study. In an earlier study published by Kimpinski and colleagues (1997) a different neurotropin, nerve growth factor (NGF), was shown to stimulate an increase in the elongation of distal neurites in both neonatal and adult sensory neurons (Kimpinski et al. 1997). This leads us to believe that HDAC is switching on groups of neurotropin genes that could lead to longer neurites and a greater neural area.

Another possible mechanism leading to the increased neural network is VPA's ability to regulate the GSK3 pathway. VPA has been shown to prolong NPC proliferation through phosphorylation of GSK-3β (Go et al. 2012). The GSK3 pathway is also regulated by BDNF and the NMDA receptor. As described above, exposure to VPA leads to overexpression of both BDNF and the NMDA receptor (Rinaldi et al. 2007; Yoo et al. 2002).

VPA may also regulate Wnt expression by regulating chromatin methylation. Prenatal exposure to VPA causes demethylation in the promotor regions of Wnt1 and Wnt2 which increases mRNA and protein levels in the cortical regions of offspring. This leads to increased levels of β-catenin which, as discussed, can affect the GSK3 pathway and neurogenesis (Go et al. 2012). The findings of this study support all the mechanisms, described above, that lead to increased neurogenesis and neurite outgrowth from exposure to VPA. These findings also support the hypothesis that VPA, as an HDAC inhibitor, leads to neurons in the cortical areas of the brain to become hyper-excitable. These findings may also bring into question as to whether other pharmaceuticals that act as HDAC inhibitors could have the same effects on a developing fetus when exposed *in utero*. Overall, our results and those of others align with the theory of an "intense world" (Markram et al. 2007) in which hyper-functioning microcircuits in the brain regulate many physical and behavioral characteristic of ASD in children.

REFERENCES

Akhtar M, Raingo J, Nelson E, Montgomery R, Olson E, Kavalali E, Monteggia L. 2009 Jun 24. Histone Deacetylases 1 and 2 Form a Developmental Switch That Controls Excitatory Synapse Maturation and Function. [accessed 2017 Jul 21]. https://www.ncbi.nlm.nih.gov/pmc/articles/PMC2895817/

Autism Speaks. 2015 Nov 13. New government survey pegs autism prevalence at 1 in 45. [accessed 2017 Jul 18]. https://www.autismspeaks.org/

Autism Society. 2016. What is Autism? [accessed 2017 Jul 18]. http://www.autism-society.org/

Berger. 2007. The complex language of chromatin. [accessed 2017 Jul 21];447. https://www.ncbi.nlm.nih.gov/pubmed/17522673

CDC 2015. 2015 Feb 26. ASD signs and symptoms. [accessed 2017 Jul 18]. https://www.cdc.gov/

Chomiak T, Turner N, Hu B. 2013 Oct 17. What we have learned about autism spectrum disorder from valproic acid. [accessed 2017 July 17]. 2013:1–8. https://www.hindawi.com/journals/pri/2013/712758/

Cohen, Stanley, Rita Levi-Montalcini, and Viktor Hamburger. 1954 Jun 29. A Nerve Growth-Stimulating Factor Isolated From Sarcomas 37 and 180. Publication. Department of Zoology, Washington University. [Accessed August 11, 2017]. http://www.pnas.org/content/40/10/1014.short.

Definition of neurite. [accessed 2017 Aug 9]. collinsdictionary.com

DiLiberti J, Farndon P, Dennis N, Curry C. 1984 Nov. The fetal valproate syndrome. [accessed 2017 Aug 9];19(3):473–481. https://www.ncbi.nlm.nih.gov/pubmed/6439041

Ebert D, Greenberg M. 2013 Jan 16. Activity-dependent neuronal signaling and autism spectrum disorder. [accessed 2017 Aug 9]:327–337. https://www.ncbi.nlm.nih.gov/pubmed/23325215

Go H, Kim K, Chang C, Jeon S, Kwon K, Han S, Lee J, Cheong J, Ryu J, Kim C, Ko K, Shin C. 2012 Nov. Prenatal exposure to valproic acid increases the neural progenitor cell pool and induces macrocephaly in rat brain via a mechanism involving the GSK-3β/β-catenin pathway. [accessed 2017 Jul 19];63(6):1028–1041. http://www.sciencedirect.com/science/article/pii/S0028390812003644

Haberland M, Montgomery R, Olson E. 2009 Jan. The many roles of histone deacetylases in development and physiology: implications for disease and therapy. [accessed 2017 Jul 20]:32–41. https://www.ncbi.nlm.nih.gov/pubmed/19065135

Harrison, Ross. 1910. The outgrowth of the nerve fiber as a mode of protoplasmic movement. Technical paper. Comparative Anatomy, Yale University. [accessed 2017 Aug 9]. http://onlinelibrary.wiley.com/doi/10.1002/jez.1400090405/full.

Horch H, Katz L. 2002 Sep 30. BDNF release from single cells elicits local dendritic growth in nearby neurons. [accessed 2017 Aug 2]:1177–1184. https://www.ncbi.nlm.nih.gov/pubmed/12368805

Jeong M, Hashimoto R, Senatorov V, Fujimaki K, Ren M, Lee M, Chuang D. 2003 Apr 11. Valproic acid, a mood stabilizer and anticonvulsant, protects rat cerebral cortical neurons from spontaneous cell death: a role of histone deacetylase inhibition. [accessed 2017 Jul 19];542(1-3):74–78. http://onlinelibrary.wiley.com/doi/10.1016/S0014-5793(03)00350-8/pdf

Kataoka S, Takuma K, Hara Y, Maeda Y, Ago Y, Matsuda T. 2013 Feb. Autism-like behaviours with transient histone hyperacetylation in mice treated prenatally with valproic acid. [accessed 2017 Aug 1];16:91–103. (1). https://www.ncbi.nlm.nih.gov/pubmed/22093185

Kimpinski K, Campenot R, Mearow K. 1997 Oct 1. Effects of the neurotrophins nerve growth factor, neurotrophin-3, and brain-derived neurotrophic factor (BDNF) on neurite growth from adult sensory neurons in compartmented cultures. Journal of Neurobiology. [accessed 2017 July 20];33(4):395-410. http://europepmc.org/abstract/med/9322157

Krames E. 2014 Mar 18. The Role of the Dorsal Root Ganglion in the Development of Neuropathic Pain. [accessed 2017 Jul 21];15(10):1669–1685. http://onlinelibrary.wiley.com/doi/10.1111/pme.12413/abstract

Laegreid L, Kyllerman M, Hedner T, Hagberg B, Viggedahl G. 1993. Benzodiazepine amplification of valproate teratogenic effects in children of mothers with absence epilepsy. [accessed 2017 Jul 18];24(2):88–92. https://www.thieme-connect.com/products/ejournals/abstract/10.1055/s-2008-1071520

Letourneau, Paul. 1975 May. Cell-to-substratum adhesion and guidance of axonal elongation. Report. Department of Biological sciences, Stanford University. [accessed 19 July, 2017]. http://www.sciencedirect.com/science/article/pii/0012160675903796.

Levi-Montalcini, Rita. 1964 Oct. The nerve growth factor. ANNALS of the New York Academy of Sciences. [accessed 2017 Jul 25];118:149-70. http://onlinelibrary.wiley.com/doi/10.1111/j.1749-6632.1964.tb33978.x/full.

MacDonald J, Roskams J. 2008 Jul 23. Histone deacetylases 1 and 2 are expressed at distinct stages of neuro-glial development. [accessed 2017 Jul 20];237(8):2256–2267. http://onlinelibrary.wiley.com/doi/10.1002/dvdy.21626/full

Markram H, Rinaldi T, Markram K. 2007 Oct 15. The Intense World Syndrome – an alternative hypothesis for autism. [accessed 2017 Jul 18]. https://www.ncbi.nlm.nih.gov/pmc/articles/PMC2518049/

Martin C, Zhang Y. 2005 Nov. The diverse functions of histone lysine methylation. [accessed 2017 Jul 21]:838–849. https://www.ncbi.nlm.nih.gov/pubmed/16261189

McGill. 2013. The Growth Cone. The Brain from Top to Bottom. [accessed 2017 Aug 11]. thebrain.mcgill.ca

Mosammaparast N, Shi Y. 2010. Reversal of Histone Methylation: Biochemical and Molecular Mechanisms of Histone Demethylases. [accessed 2017 Jul 21];79:155–179. https://www.ncbi.nlm.nih.gov/pubmed/20373914

Phiel C, Zhang F, Huang E, Guenther M, Lazar M, Klein P. 2001 Sep 28. Histone Deacetylase Is a Direct Target of Valproic Acid, a Potent Anticonvulsant, Mood Stabilizer, and Teratogen. [accessed 2017 Jul 20]. https://www.ncbi.nlm.nih.gov/pubmed/11473107

Purves D, Augustine GJ, Fitzpatrick D. 2001. Neuroscience. 2nd edition. Sunderland (MA): Sinauer Associates. The Axonal Growth Cone. https://www.ncbi.nlm.nih.gov/books/NBK11114

Rasalam AD, Hailey H, Williams JHG, Moore SJ. 2005 Aug. Characteristics of fetal anticonvulsant syndrome associated autistic disorder. [accessed 2017 Aug 9];47(8):551–555. https://www.ncbi.nlm.nih.gov/pubmed/16108456

Rinaldi T, Kulangara K, Antoniello K, Markram H. 2007 Aug 14. Elevated NMDA

receptor levels and enhanced postsynaptic long-term potentiation induced by prenatal exposure to valproic acid. [accessed 2017 Aug 2]. http://www.pnas.org/content/104/33/13501

Schneider T, Przewlocki R. 2004 Jul 7. Behavioral Alterations in Rats Prenatally Exposed to Valproic Acid: Animal Model of Autism. [accessed 2017 Jul 19]. https://www.ncbi.nlm.nih.gov/pubmed/15238991

Smith Y. 2015 July 20. Valproic Acid Pharmacology. News Medical Life Sciences. [accessed 2017 Jul 19]. https://www.news-medical.net/health/Valproic-Acid- Pharmacology.aspx

Tung E, Winn L. 2010 Nov 1. Epigenetic modifications in valproic acid-induced teratogenesis. [accessed 2017 Jul 21];248(3):201–209. https://www.ncbi.nlm.nih.gov/pubmed/20705080

Wiens D, DeWitt A, Kosar M, Underriner C, Finsand M, Freese M. 2016 May 3. Influence of Folic Acid on Neural Connectivity during Dorsal Root Ganglion Neurogenesis. [accessed 2017 Aug 1]. https://www.ncbi.nlm.nih.gov/pubmed/27160668

Yoo, Min, Tae-Youn Kim, Young Yoon, Jae-Young Koh. 2016 Jun 29. Autism phenotypes in ZnT3 null mice: Involvement of zinc dyshomeostasis, MMP-9 activation and BDNF upregulation. Scientific reports-nature search journal. [accessed 2017 Aug 2]. https://www.nature.com/articles/srep28548

APPENDIX A

HISTOGRAMS

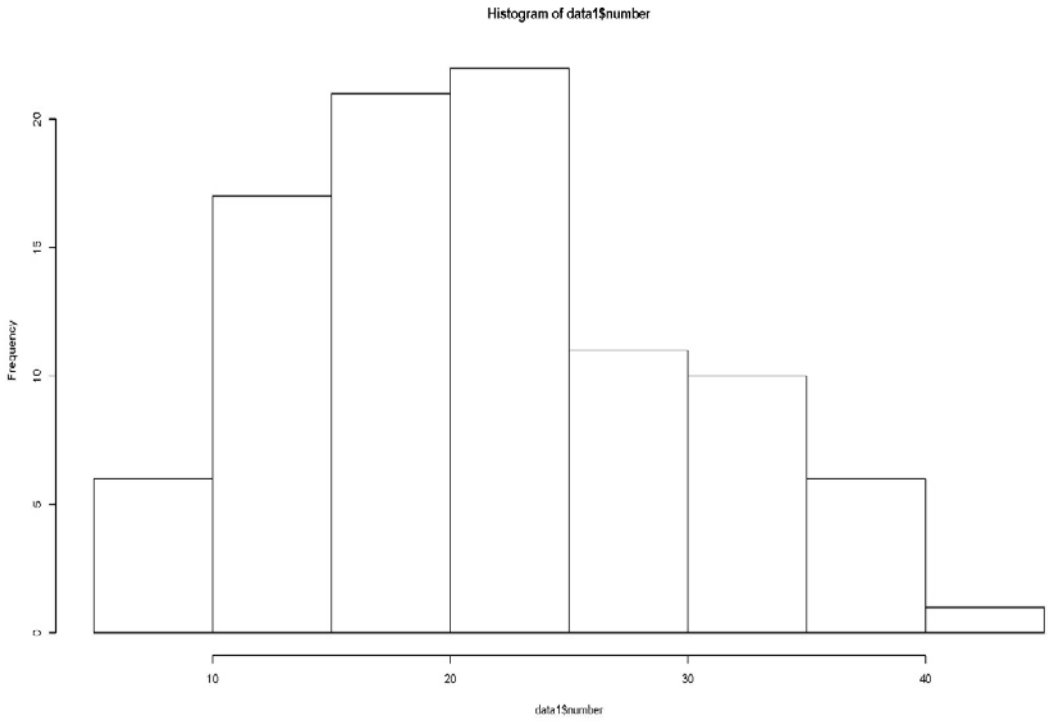

Figure A1. Histogram of neurite number data showing normal distribution

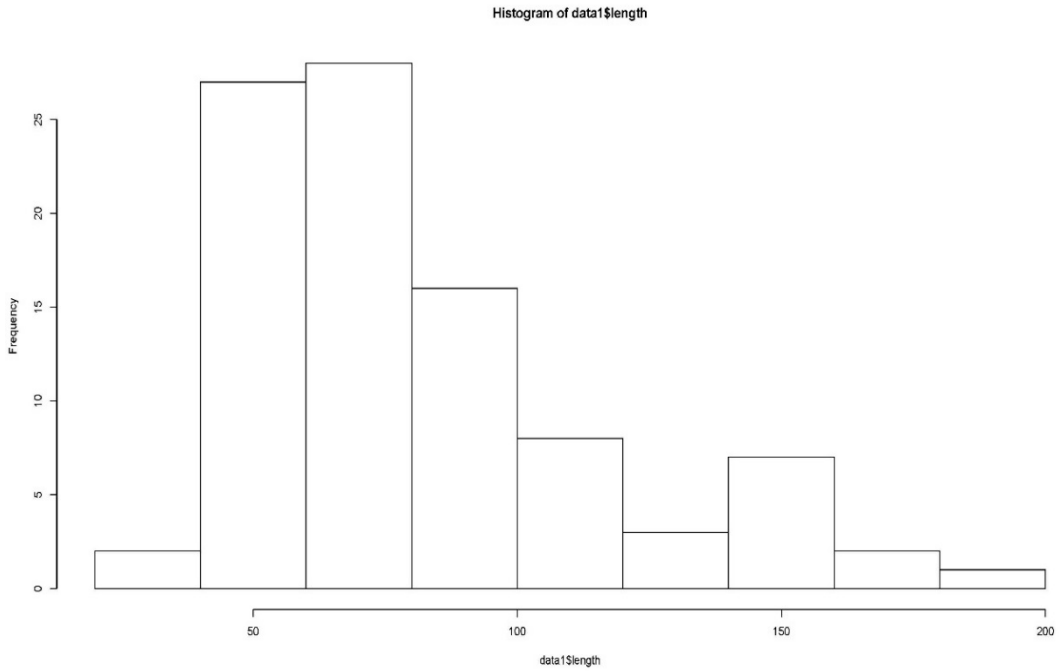

Figure A2. Histogram of neurite length data showing not normal distribution

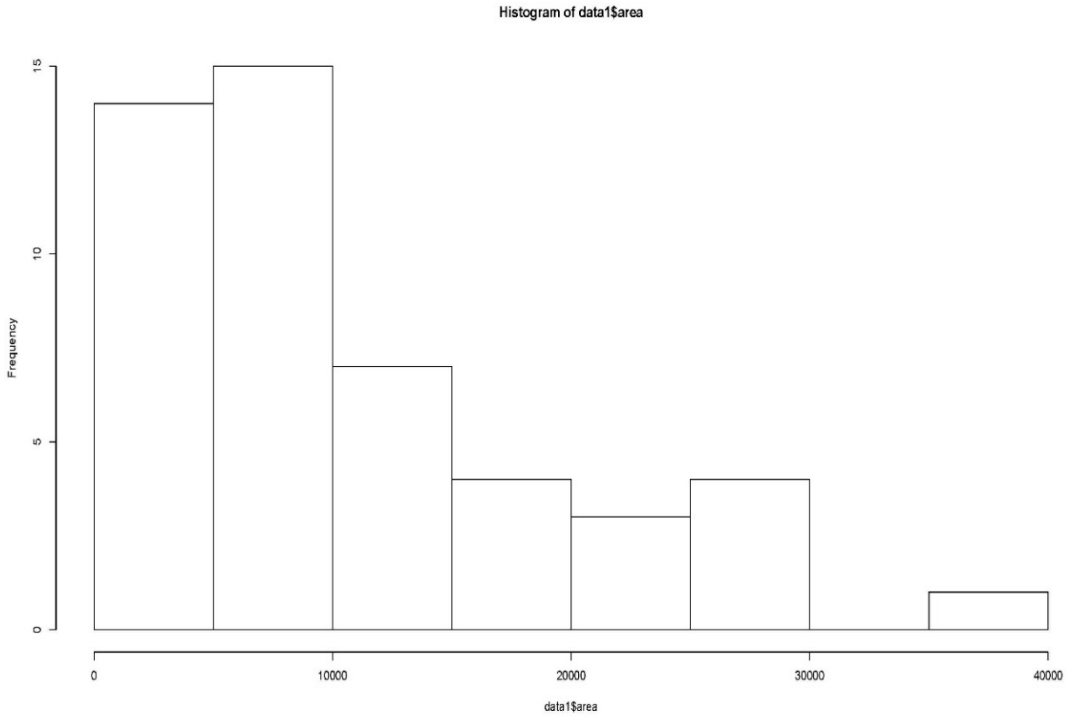

Figure A3. Histogram of synaptogenic area showing data to be not normally distributed

APPENDIX B

COMPLETE DATA SETS

Table B1. Average, median, minimum, and maximum DRG neurite number. Numbers listed are a representation of total averages

	Average	Median	Minimum	Maximum
Control	16.09667	15	7	29
50 µM	22.75	22.5	10	36
100 µM	25.83333	25	12	42
200 µM	24.9	23.5	13	35
300 µM	22.66667	23	10	30

.

Table B2. Average, median, minimum, and maximum DRG neurite length. Numbers listed are a representation of total averages.

	Average (µm)	Median (µm)	Minimum (µm)	Maximum (µm)
Control	53.98859	49.747	38.68414	83.4627
50 µM	70.57807	64.66285	50.23535	102.0684
100 µM	111.802	108.2713	50.33595	193.2348
200 µM	74.08639	71.08172	47.17987	98.751
300 µM	70.75712	66.9584	66.9584	94.73465

Table B3. Average, median, minimum, and maximum DRG synaptogenic area. Numbers listed are a representative of total averages.

	Average (µm)	Median (µm)	Minimum (µm)	Maximum (µm)
Control	8112.56701	5773.16737	622.059195	26005.6752
50 µM	10641.0942	8651.62218	2723.09832	26768.0041
100 µM	12118.7537	5988.66905	2942.61006	37535.6902
200 µM	10039.9141	7361.0218	2322.1984	22191.9767
300 µM	13148.7849	10713.8654	4867.71738	28075.8222

APPENDIX C

SIGNIFICANCE TESTING DATA SETS

Table C1. Significance values as determined by the T-TEST for neurite number. Each treated explant compared to the control and to each other. Bolded values indicate significance with $p \leq 0.05$.

	50 µM	100 µM	200 µM	300 µM
Control	0.065764	**2.73536^-7**	**0.002113**	**0.010594**
50 µM		0.373373	0.567203	0.981834
100 µM			0.715126	0.205093
200 µM				0.44674

Table C2. Significance values as determined by the Wilcoxon Rank Sum Test for neurite length. Each treated explant compared to the control and to each other. Bolded values indicate significance with $p \leq 0.05$.

	50 µM	100 µM	200 µM	300 µM
Control	**0.005272**	**8.636×10^{-14}**	**.0005786**	**0.001416**
50 µM		**0.0008243**	0.4598	0.9626
100 µM			**0.001064**	**0.0002873**
200 µM				0.6607

C3. Significance values as determined by the Wilcoxon Rank Sum Test for synaptogenic area. Each treated explant compared to the control and to each other. Bolded values indicate significance with $p \leq 0.05$.

	50 µM	100 µM	200 µM	300 µM
Control	0.1728	0.2799	0.4262	**0.04347**
50 µM		0.8286	0.7168	0.3704
100 µM			0.8633	0.2775
200 µM				0.2947